

# Relating the Neural Representations of Vocalized, Mimed, and Imagined Speech

Maryam Maghsoudi<sup>1</sup>, Rupesh Chillale<sup>1</sup>, Shihab A. Shamma<sup>1</sup>

<sup>1</sup> University of Maryland - College Park, United States

maryam00@umd.edu, rupesh.chillale@ahduni.edu.in, sas@umd.edu

## Abstract

We investigated the relationship among neural representations of vocalized, mimed, and imagined speech recorded using publicly available stereotactic EEG recordings. Most prior studies have focused on decoding speech responses within each condition separately. Here, instead, we explore how responses across conditions relate by training linear spectrogram reconstruction models for each condition and evaluate their generalization across conditions. We demonstrate that linear decoders trained on one condition generally transfer successfully to others, implying shared speech representations. This commonality was assessed with stimulus-level discriminability by performing a rank-based analysis demonstrating preservation of stimulus-specific structure in both within- and across-conditions. Finally, we compared linear reconstructions to those from a nonlinear neural network. While both exhibited cross-condition transfer, linear models achieve superior stimulus-level discriminability.

**Index Terms:** speech decoding, neural representations, brain-computer interface

## 1. Introduction

Understanding how neural responses to speech reflect its phonetic, syllabic, and semantic features is a central aim of auditory neuroscience, providing insights into both the processing of speech in the brain, and the development of brain-computer interfaces (BCI) [1]. Numerous studies have attempted to decode speech and its features from invasive and non-invasive brain responses to external auditory stimuli, i.e., during *listening* to speech. For example, most prior work has reconstructed speech spectrograms from auditory cortical activity and identified phonetic feature encoding during passive listening [2, 3, 4]. But recent reports have demonstrated high-fidelity reconstruction and synthesis of overt speech from neural responses recorded during speech vocalization [5], an experimental condition that is important for advances in BCI and for elaborating the internal processes to produce speech vocalization, such as planning and motor articulation [6, 7].

In addition to vocalized speech, two additional forms of speech are relevant for understanding internal speech processes: mimed and imagined speech. Mimed speech involves articulatory planning and motor execution without overt acoustic output or auditory feedback. Imagined speech, more accurately imagining to speak, reflects internal generative and planning processes without overt motor movement or acoustic output. Recent work has investigated decoding from mimed [8] and imagined speech [9, 10, 11]. These studies demonstrated that silent articulation and attempted speech contain structured neural information sufficient for decoding. These two conditions are even more important in BCI applications, as they address

individuals without the ability to produce speech. Note that decoding imagined speech presents additional challenges due to the absence of external timing cues, which complicates alignment between neural activity and speech features [12].

In this work, in addition to decoding speech from these three conditions, we are specifically interested in neural representation similarities among them. Prior work has reported overlapping neural activity between overt and imagined speech [13, 14] motivating investigation of their representational similarity and suggesting that decoders trained on one condition may generalize to others. For instance, a decoder trained within one condition learns a mapping between neural activity patterns and its acoustic features. But when applied to a different condition, its performance would depend on the extent to which the underlying neural representations are shared between the two.

Here we shall use a publicly available stereotactic EEG dataset containing recordings of vocalized, mimed, and imagined speech of a single participant [15]. We *first* fit linear decoders separately for each condition and evaluate reconstruction performance within each condition. *Second*, we perform cross-condition evaluation to test whether decoders trained in one case can be applied to the others. In this part, we also evaluate whether there is shared neural representational similarity between the three conditions that allows for such decoder transfer. *Third*, to evaluate how much stimulus-specific information is preserved during speech reconstruction, we perform a rank-based analysis to measure stimulus-specific discriminability in reconstructed speech. While reconstruction correlation provides a measure of overall similarity between predicted and target speech features, it does not directly quantify whether stimulus-specific structure is preserved. For this reason, it is important to complement correlation-based evaluation with analyses that assess stimulus-level individuality. *Fourth*, linear models are known to be more interpretable, which allows for reasoning about possible shared neural representations. Moreover, recent work has shown that linear decoders can perform competitively with nonlinear architectures in reconstructing speech acoustics from neural signals [16]. To examine whether these results are consistent across different decoder architectures, we perform the same analyses using a nonlinear decoder introduced in prior work [15], which uses convolutional and recurrent layers for spectrogram reconstruction. Therefore, altogether this work presents an investigation of the relationships among neural representations of three speech modes of production (vocalized, mimed, and imagined) that may further help with a deeper understanding of the process, and eventually with BCI applications.

## 2. Methods

### 2.1. Dataset

We used the publicly available VocalMind dataset [15], which includes stereotactic EEG (sEEG) recordings from a single participant during vocalized, mimed, and imagined speech in Mandarin Chinese. The dataset contains 100 sentences, each repeated twice per condition. We used the published preprocessed signals from 110 electrodes (low-pass filtered at 100 Hz). For stimulus representation, we used the provided vocalized audio recordings and computed time–frequency features using the NSL cortical model [17] which mimics the processing of the human cochlea by transforming the acoustic waveform into a biologically motivated time–frequency representation.

### 2.2. Linear reconstruction model

We trained linear decoders to reconstruct the stimulus spectrogram from time-lagged sEEG responses. The reconstructed spectrogram value at time  $t$  and frequency  $f$  is given by:

$$\hat{S}(t, f) = \sum_c \sum_{l \in L} g(c, l, f) X(t - l, c) \quad (1)$$

where  $g(c, l, f)$  are the model weights for each channel  $c$ , lag  $l$ , and frequency  $f$ , and  $X(t - l, c)$  is the neural response at channel  $c$  lagged by  $l$ .  $L$  represents the set of all lags used.

In matrix form, the above equation can be written as  $\hat{S} = G^T X_{\text{lag}}$ , and the solution is given by:

$$G = \arg \min_G \|S - G^T X_{\text{lag}}\|_F^2 + \alpha \|G\|_F^2 \quad (2)$$

The regularization parameter  $\alpha$  was selected using grid search to prevent overfitting. We split the dataset into training and test sets and fit  $G$  separately for each condition (Vocalized, Mimed, and Imagined), yielding transfer functions called  $G_v$ ,  $G_m$ , and  $G_i$ .

To assess statistical significance of these models, we fit null models by shuffling the trial orders, thereby pairing sEEG responses with mismatched spectrograms, resulting in  $G_{v\text{-null}}$ ,  $G_{m\text{-null}}$ , and  $G_{i\text{-null}}$ . All other computations were kept the same.

### 2.3. Non-linear reconstruction model

We retrained the model introduced in the VocalMind study [15] to decode mel-spectrograms from sEEG signals. The architecture includes a convolutional block for feature extraction followed by a recurrent (RNN) block that captures temporal dependencies (Figure 1, left). Mean squared error (MSE) loss is used during training. The estimated mel-spectrogram can be converted into speech using a pre-trained HiFi-GAN model [18].

Training was performed separately for Vocalized, Mimed, and Imagined responses, producing reconstructed spectrograms for each condition, from which envelopes are computed. These reconstructions are evaluated using the same metrics described in the following section, allowing comparison between linear and nonlinear approaches.

### 2.4. Evaluation

We evaluate cross-condition generalization to assess how well decoders transfer across speaking conditions. In cross-condition evaluation, the model is trained on one condition and tested on the held-out data from the same condition as well as

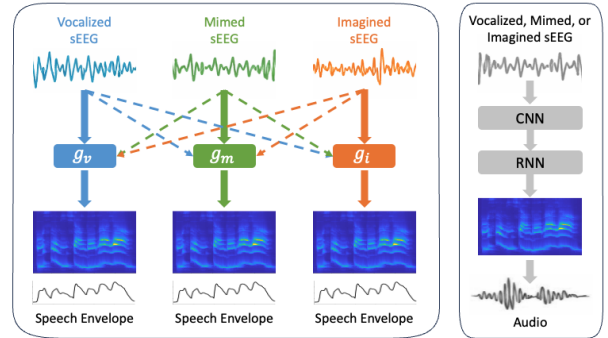


Figure 1: *Linear and nonlinear decoding approaches. Left: Condition-specific linear decoders are trained on Vocalized, Mimed, or Imagined sEEG and evaluated both within and across conditions. Right: Nonlinear neural network architecture used for spectrogram reconstruction in [15].*

the other two conditions (Figure 1, left). To measure the similarity between the reconstructed and the target spectrograms, we compute the linear correlation between them. Additionally, we compute the spectrogram envelope by averaging over the frequency axis and measure the linear correlation between reconstructed and target envelopes. We compare these correlation values with those obtained from null models and measure statistical significance.

To see how well the sentence-level discriminability is preserved in the reconstructed spectrograms, we perform rank analysis. For each reconstructed spectrogram, the envelope is computed and is correlated with all candidate target envelopes. For each  $k$  we ask the question: In how many cases does the correct sentence appear within the top- $k$  matches? We plot the top- $k$  curve and compare it to chance, where  $chance = \frac{k}{N}$  and  $N$  is the total number of sentences. An early large gap between the top- $k$  curve and chance shows stronger sentence-specificity. We evaluate the significance by computing the difference in the area under curve (AUC) of the top- $k$  curve and the chance line.

$$AUC = \sum_{k=1}^N (\text{Top}_k(k) - \frac{k}{N}) \quad (3)$$

Higher AUC values indicate stronger sentence-level discriminability in the reconstructed signals.

## 3. Results

### 3.1. Cross-condition reconstruction performance

We evaluate speech envelope reconstruction within and across conditions. In the within-condition setting,  $G_{\text{condition}}$  is applied to held-out test sentences from the same condition. In the cross-condition setting,  $G_{\text{condition}}$  is applied to the other two conditions (e.g.,  $G_m$  applied to  $X_v$  and  $X_i$ ). Reconstruction performance is quantified using linear correlations between reconstructed and target spectrogram envelopes. In all cases, correlation distributions significantly exceed their corresponding null distributions (all  $p \ll 0.001$ ), generated using  $G_{v\text{-null}}$ ,  $G_{m\text{-null}}$ , and  $G_{i\text{-null}}$ .

Figure 2 (left) summarizes cross-condition performance for linear models. The Vocalized-trained decoder ( $G_v$ ) achieves the highest performance on Vocalized data ( $p \ll 0.001$ ), followed by Mimed and then Imagined data, indicating progressively re-

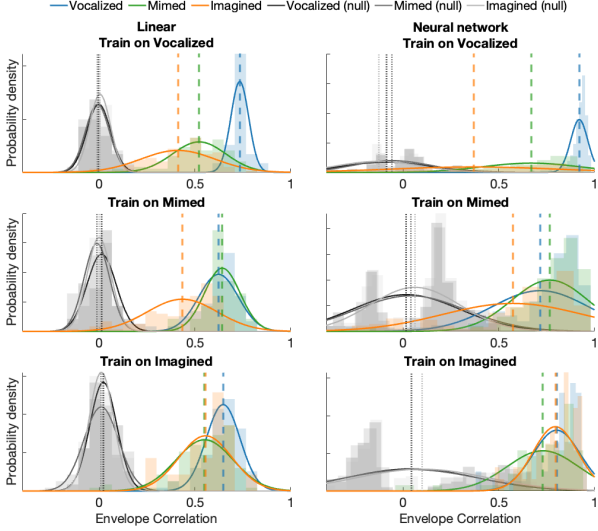


Figure 2: Envelope correlation distributions for linear (left) and neural network (right) decoders. Rows indicate training condition. Colored curves show performance across test conditions; gray distributions represent null models obtained by shuffling. Dashed lines mark mean correlations.

duced transfer as articulatory and sensory components are removed.

For the Mimed-trained decoder ( $G_m$ ), performance on Mimed and Vocalized data does not differ significantly ( $p = 0.6$ ), while both exceed performance on Imagined speech ( $p \ll 0.001$ ). This indicates strong shared articulatory-related structure between Mimed and Vocalized conditions, with reduced overlap for Imagined speech.

For the Imagined-trained decoder ( $G_i$ ), performance is highest on Vocalized data ( $p \ll 0.005$ ) and comparable between Imagined and Mimed conditions. Although this ordering may appear counterintuitive, it indicates that the additional neural processes present during Vocalized speech do not obscure the planning-related information learned from Imagined speech, and may even preserve it.

Overall, Mimed-trained decoders treat Mimed and Vocalized similarly, while Imagined-trained decoders treat Imagined and Mimed similarly. This supports the view that Mimed speech occupies an intermediate representational position between Vocalized and Imagined speech, sharing articulatory-related structure with the former and planning-related structure with the latter.

### 3.2. A linear explanation for cross-condition transfer

Let  $X_{\text{lag}}$  denote the neural response matrix used for decoding. We assume neural activity can be decomposed into components reflecting different processing stages: Imagined speech primarily contains internal planning or generative processes ( $X_P$ ), Mimed speech contains planning plus articulatory activity ( $X_P + X_A$ ), and Vocalized speech contains planning, articulatory, and sensory/feedback-related components ( $X_P + X_A + X_S$ ). Formally,

$$X_V = X_P + X_A + X_S, \quad X_M = X_P + X_A, \quad X_I = X_P. \quad (4)$$

The linear decoder is  $\hat{S} = G^T X_{\text{lag}}$ , where  $G$  is learned from a single training condition. Because  $G_{\text{train}}$  is optimized only on

that condition, it captures neural directions that are predictive within that training regime. Geometrically, the decoder defines a neural subspace used to reconstruct the stimulus, and cross-condition generalization depends on how much test-condition activity projects onto this learned subspace (i.e., subspace overlap).

For a Mimed-trained decoder (trained on  $X_M = X_P + X_A$ ), applying it to Vocalized responses gives

$$\begin{aligned} \hat{S}_{M \rightarrow V} &= G_M^T X_V = G_M^T (X_P + X_A + X_S) \\ &= \underbrace{G_M^T (X_P + X_A)}_{\hat{S}_{M \rightarrow M}} + G_M^T X_S, \end{aligned} \quad (5)$$

so,  $\hat{S}_{M \rightarrow V} - \hat{S}_{M \rightarrow M} = G_M^T X_S$ . Thus,  $M \rightarrow V$  is similar to  $M \rightarrow M$  when the additional Vocalized-specific component  $X_S$  has small projection onto the predictive subspace captured by  $G_M$ . In contrast, applying the same decoder to Imagined speech yields

$$\hat{S}_{M \rightarrow I} = G_M^T X_I = G_M^T X_P, \quad (6)$$

and relative to Mimed testing,  $\hat{S}_{M \rightarrow M} - \hat{S}_{M \rightarrow I} = G_M^T X_A$ , predicting  $M \rightarrow M \approx M \rightarrow V > M \rightarrow I$  when  $X_A$  contributes to stimulus prediction.

For an Imagined-trained decoder (trained only on  $X_I = X_P$ ), additional components present in Mimed and Vocalized speech ( $X_A, X_S$ ) are not explicitly learned during training, but they can still influence reconstruction if they overlap with the planning subspace. To make this precise, decompose  $X_A = X_A^{\parallel} + X_A^{\perp}$  and  $X_S = X_S^{\parallel} + X_S^{\perp}$ , where the  $\parallel$  components lie in the imagined/planning subspace and the  $\perp$  components are orthogonal to it. Because  $G_I$  is learned from  $X_P$ , it primarily acts on directions within this subspace, implying  $G_I^T X_A = G_I^T X_A^{\parallel}$  and  $G_I^T X_S = G_I^T X_S^{\parallel}$ .

Thus, articulatory and sensory activity contribute to reconstruction only to the extent that they project onto planning-related directions. If these projections are substantial, the Imagined-trained decoder can generalize to Mimed (and potentially Vocalized) speech; if not, performance drops.

### 3.3. Sentence-level discriminability

While envelope correlation captures overall reconstruction similarity, it does not directly measure preservation of sentence-specific structure. To evaluate discriminability, we perform rank analysis between reconstructed and target envelopes and compute the AUC above chance for the top- $k$  curves for each trained model ( $G_v, G_m, G_i$ ) applied to each condition ( $X_v, X_m, X_i$ ).

Sentence-level discriminability is strongest when models are tested on Vocalized responses. The highest AUC is obtained for  $G_v$  applied to  $X_v$  (AUC = 0.32). When  $G_m$  and  $G_i$  are applied to  $X_v$ , performance remains above chance, indicating preserved sentence-specific structure in Vocalized data.

For the Mimed-trained decoder, performance on  $X_v$  and  $X_m$  is similar (AUC = 0.11 and 0.13) and substantially lower on  $X_i$  (AUC = -0.01).

For the Imagined-trained decoder, performance on  $X_i$  and  $X_m$  is comparable (AUC = 0.07 and 0.08), and lower overall relative to Vocalized testing.

Overall, the rank analysis shows the same transfer structure observed in reconstruction correlations: Mimed-trained decoders treat Mimed and Vocalized similarly, while Imagined-trained decoders treat Imagined and Mimed similarly. This sup-

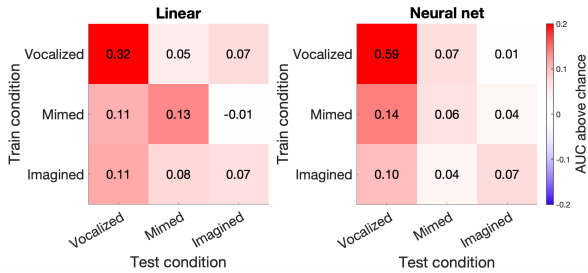


Figure 3: Sentence-level discriminability measured by AUC above chance for linear (left) and neural network (right) decoders. Positive values (red) reflect performance above chance.

ports the view that Mimed speech occupies an intermediate representational position between Vocalized and Imagined speech.

### 3.4. Non-linear neural network decoder

We next evaluate cross-condition reconstruction performance using the nonlinear neural network model. Figure 2 (right) shows reconstructed envelope correlations for each training–test pairing. Null models were trained with temporally circularly shifted target spectrograms. The nonlinear model significantly outperforms null in both within- and cross-condition settings (all  $p \ll 0.001$ ), indicating reliable transfer across conditions.

When trained on Vocalized speech, the model achieves its highest performance on Vocalized responses and remains significantly above null for Mimed and Imagined speech ( $p \ll 0.001$ ), though reduced relative to the within-condition case.

For the Mimed-trained model, performance on Mimed and Vocalized responses remains close ( $p = 0.02$ ,  $d = 0.16$ ), with both exceeding performance on Imagined speech, consistent with shared structure between Vocalized and Mimed activity.

For the Imagined-trained model, performance is comparable between Vocalized and Imagined responses ( $p = 0.74$ ,  $d = 0.04$ ) and lower on Mimed speech ( $p = 0.02$ ,  $d = 0.29$ ). Overall, the nonlinear model shows a similar transfer pattern to the linear model, with a difference in the Imagined-trained case.

To assess sentence-level discriminability, we apply the same rank analysis used in the linear framework. Figure 3 (right) shows AUC above chance for the nonlinear model. Training and testing on Vocalized speech yields the highest AUC (0.59), and testing on Vocalized responses consistently produces the strongest discriminability across all training conditions. For the Mimed-trained network, performance is highest on Vocalized responses (AUC = 0.14), followed by Mimed (AUC = 0.06), and lowest on Imagined speech (AUC = 0.04). Similarly, for the Imagined-trained network, performance is highest on Vocalized responses (AUC = 0.10), with lower and more comparable values on Imagined and Mimed speech (AUC = 0.07 and 0.04).

Overall, although the nonlinear model achieves higher reconstruction correlations ( $p \ll 0.005$ ), its rank analysis differs from the pattern observed in the linear model. This difference motivated us to examine whether higher correlation necessarily implies stronger sentence-level discriminability. As shown in Figure 4, AUC increases with mean reconstruction correlation for both models; however, the linear model exhibits a steeper relationship (Steiger’s test,  $p = 1.24 \times 10^{-4}$ ). Improvements in reconstruction accuracy therefore do not translate into proportional gains in sentence-level separation, and in this setting, the linear model better preserves sentence-specific structure.

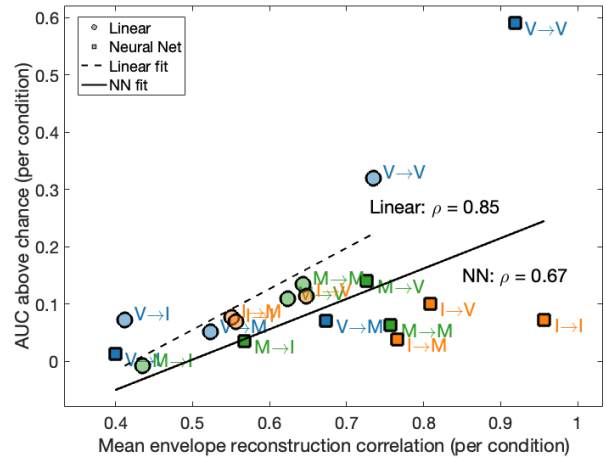


Figure 4: Relationship between mean envelope reconstruction correlation and sentence-level discriminability for linear and neural network decoders. Each point represents a training–test pair (circles: linear; squares: neural network). Dashed and solid lines show the corresponding linear fits.

## 4. Discussion

Our results are consistent with the hierarchical relationship hypothesis between neural responses to Imagined, Mimed, and Vocalized speech, with imagined containing planning-related activity, mimed containing planning and articulatory components, and vocalized containing planning, articulatory, and auditory feedback components. Future research could use subspace analyses, such as comparing principal components or computing subspace alignment between speech conditions, to directly test this hypothesis. Additionally, future work would benefit from incorporating neural recordings during listened speech to evaluate the auditory sensory feedback component hypothesized to be present during vocalization. Finally, our comparison of linear and nonlinear models shows the importance of interpretability when using nonlinear decoders. Future work can further investigate this to better understand which neural components support cross-condition generalization.

## 5. Conclusion

We demonstrated that linear decoders can map sEEG responses to acoustic spectrograms during vocalized, mimed, and imagined speech. When applied cross-conditionally, these decoders still perform significantly above chance, suggesting that neural responses across speech modes share a common structure. We observed transfer patterns consistent with a hierarchical representational organization, where imagined speech engages a subset of processes present in mimed speech, and mimed speech engages a subset of those present in vocalized speech. Rank analysis also showed that stimulus-specific discriminability is preserved above chance in the reconstructions. We also showed that a nonlinear neural network achieves similar cross-condition transfer and above-chance discriminability. However, comparing the linear and nonlinear models demonstrated stronger preservation of stimulus-specific structure in the linear case, emphasizing the importance of interpretability when evaluating neural decoding performance.

## 6. Acknowledgement

This work is supported in part by a grant from the Airforce Office of Scientific Research and NIH R01-DC005779 to SAS.

## 7. Generative AI Use Disclosure

Generative AI tools were used for language editing and minor phrasing refinement. All scientific content and conclusions were developed by the authors.

## 8. References

- [1] J. G. Makin, D. A. Moses, and E. F. Chang, "Machine translation of cortical activity to text with an encoder–decoder framework," *Nature Neuroscience*, vol. 23, pp. 575–582, 2020.
- [2] N. Mesgarani, C. Cheung, K. Johnson, and E. F. Chang, "Phonetic feature encoding in human superior temporal gyrus," *Science*, vol. 343, no. 6174, pp. 1006–1010, 2014.
- [3] B. N. Pasley, S. V. David, N. Mesgarani *et al.*, "Reconstructing speech from human auditory cortex," *PLoS Biology*, vol. 10, no. 1, p. e1001251, 2012.
- [4] H. Akbari, B. Khalighinejad, J. L. Herrero, A. D. Mehta, and N. Mesgarani, "Towards reconstructing intelligible speech from the human auditory cortex," *Scientific Reports*, vol. 9, p. 874, 2019.
- [5] G. K. Anumanchipalli, J. Chartier, and E. F. Chang, "Speech synthesis from neural decoding of spoken sentences," *Nature*, vol. 568, no. 7753, pp. 493–498, 2019.
- [6] G. Hickok and D. Poeppel, "The cortical organization of speech processing," *Nature Reviews Neuroscience*, vol. 8, no. 5, pp. 393–402, 2007.
- [7] P. Indefrey and W. J. M. Levelt, "The spatial and temporal signatures of word production components," *Cognition*, vol. 92, no. 1–2, pp. 101–144, 2004.
- [8] S. Martin, P. Brunner, I. Iturrate *et al.*, "Decoding spectrotemporal features of overt and covert speech from the human cortex," *Journal of Neural Engineering*, vol. 11, no. 3, p. 035007, 2014.
- [9] D. A. Moses, S. L. Metzger, J. R. Liu *et al.*, "Neuroprosthesis for decoding speech in a paralyzed person with anarthria," *New England Journal of Medicine*, vol. 385, no. 3, pp. 217–227, 2021.
- [10] F. R. Willett, D. T. Avansino, L. R. Hochberg, J. M. Henderson, and K. V. Shenoy, "A high-performance speech neuroprosthesis," *Nature*, vol. 620, pp. 1031–1036, 2023.
- [11] S. Martin *et al.*, "Word pair classification during imagined speech using direct brain recordings," *Scientific Reports*, vol. 6, p. 25803, 2016.
- [12] M. Maghsoudi, M. Rezaeizadeh, and S. Shamma, "A convolutional framework for mapping imagined auditory meg into listened brain responses," *arXiv preprint arXiv:2512.03458*, 2025. [Online]. Available: <https://arxiv.org/abs/2512.03458>
- [13] X. Pei, D. L. Barbour, E. C. Leuthardt, and G. Schalk, "Spatiotemporal dynamics of electrocorticographic high gamma activity during overt and covert word repetition," *PNAS*, vol. 108, no. 10, pp. 4187–4192, 2011.
- [14] X. Tian and D. Poeppel, "Mental imagery of speech and movement implicates the dynamics of internal forward models," *Proceedings of the National Academy of Sciences*, vol. 107, no. 25, pp. 11 525–11 530, 2010.
- [15] T. He, M. Wei, R. Wang, R. Wang, S. Du, S. Cai, W. Tao, and H. Li, "Vocalmind: A stereotactic eeg dataset for vocalized, mimed, and imagined speech in tonal language," *Scientific Data*, vol. 12, no. 1, p. 657, 2025.
- [16] A. D. MacIntyre, C. Gaultier, and T. Goehring, "Decoding of speech acoustics from eeg: going beyond the amplitude envelope," *Journal of Neural Engineering*, vol. 23, no. 1, p. 016012, 2026. [Online]. Available: <https://iopscience.iop.org/article/10.1088/1741-2552/ae3ae1>
- [17] T. Chi, P. Ru, and S. A. Shamma, "Multiresolution spectrotemporal analysis of complex sounds," *The Journal of the Acoustical Society of America*, vol. 118, no. 2, pp. 887–906, 2005.
- [18] J. Kong, J. Kim, and J. Bae, "Hifi-gan: Generative adversarial networks for efficient and high fidelity speech synthesis," in *Advances in Neural Information Processing Systems*, vol. 33. Curran Associates, Inc., 2020, pp. 17 022–17 033.